IJE TRANSACTIONS A: Basics Vol. 36 No. 04, (April 2023) 615-629

International Journal of Engineering

Journal Homepage: www.ije.ir

Visible Light Activated Fe-N-SiO_2/TiO_2 Photocatalyst: Providing an Opportunity for Enhanced Photocatalytic Degradation of Antibiotic Oxytetracycline in Aqueous Solution

S. A. Habeeb[a,b], A. A. Zinatizadeh*[a,c], S. A. Mousavi[d], H. Zangeneh[e]

[a] *Department of Applied Chemistry, Faculty of Chemistry, Razi University, Kermanshah, Iran*
[b] *Pharmacy Faculty, University of Babylon, Babylon, Iraq*
[c] *Environmental and Pollution Engineering Group, Environmental Research Center (ERC), Razi University, Kermanshah, Iran*
[d] *Department of Health Engineering, Kermanshah University of Medical Sciences, Kermanshah, Iran*
[e] *Department of Chemical Engineering, Isfahan University of Technology, Isfahan, Iran*

PAPER INFO

Paper history:
Received 22 August 2022
Received in revised form 16 December 2022
Accepted 31 December 2022

Keywords:
Photocatalytic Degradation
Nonbiodegradable Antibiotics
Fe-N-SiO_2/TiO_2
Oxytetracycline

ABSTRACT

To probe advantages in Fe-N-SiO_2/TiO_2 nanocomposite system, the visible photocatalytic degradation of the nonbiodegradable antibiotic oxytetracycline (OTC) by unsupported TiO_2 and its modified composites by incorporating each of the Fe, N, and SiO_2 dopants under a series of conditions were investigated. The structural and optical properties as well as the morphology of the prepared nanocomposites were also characterized applying Fourier transform infrared (FT-IR), X-ray diffraction, photoluminescence spectroscopy, UV-visible diffuse reflectance spectra and field emission scanning electron microscopy/Energy-dispersive X-ray spectroscopy (FESEM/EDX). In order to develop two models portraying appropriate functional relationships between two main responses (OTC removal efficiency and its specific removal rate (SRR)) and four numerical variables (OTC concentration, catalysis loading, initial pH and reaction time), two separate multivariate analysis pathways under response surface methodology (RSM) were taken. The results obtained all came down to the maximum SRR (220 OTC mg $_{OTC\ removed}$/g $_{cat}$. h) found at the maximum catalyst dosage of 1.5 g/l, and acidic pH of 3 after 0.5 h. Furthermore, the Fe-N-SiO_2/TiO_2 proved a stable photocatalytic activity during three subsequent reusability experiments, shedding light on its reliable potential for future application.

***doi**: 10.5829/ije.2023.36.04a.02*

1. INTRODUCTION

As a member of one of the most commonly worldwide used classes of antibiotic chemicals aiming significantly for disease prevention and its treatment, oxytetracyclines (OTC) has been frequently detected in the environment, mostly involving water bodies [1, 2]. The environmental contamination caused by OTC is usually originated from pharmaceutical manufacture, livestock farming, and agricultural discharges [3, 4].

Due to beiextremely resistantant to biodegradation [5], a large number of studies focused on alternative non-biological processes for OTC removal [6]. Providing the opportunity of being carried out at room temperature and atmospheric pressure while obtaining high levels of mineralization of various pollutants to mainly water, CO_2, and inorganic compounds, throughout the recent decades, photocatalytic technology as an advanced oxidation process (AOP) has been showing great promise in antibiotics degradation [7]. Performing under visible light irradiation is the key to the practical application of photocatalysts. Meanwhile, TiO_2 mediated photocatalysis has been highlighted as one of the most promising approaches to degrade stable organic contaminants in water by producing hydroxyl radicals [8, 9]. Given their sufficiently optical/electric properties, non-toxic nature, high photocatalytic capacity, and long-term chemical stability, metal oxide semi-conductors

*Corresponding Author Email: zinatizadeh@gmail.com
(A. A. Zinatizadeh)

Please cite this article as: S. A. Habeeb, A. A. Zinatizadeh, S. A. Mousavi, H. Zangeneh, Visible Light Activated Fe-N-SiO_2/TiO_2 Photocatalyst: Providing an Opportunity for Enhanced Photocatalytic Degradation of Antibiotic Oxytetracycline in Aqueous Solution, ***International Journal of Engineering, Transactions A: Basics***, Vol. 36, No. 04, (2023), 615-629

including TiO_2 have been proven in recent publications as potential photocatalysts for successful oxidation as well as antibacterial inactivation of OTC [10, 11].

Possessing a large band gap (3.2 eV) limiting its activation to only ultraviolet (UV) region and low quantum efficiency caused by high e^-/h^+ recombination, TiO_2 meets a major drawback in its wide application [12]. Many efforts have been devoted to overcome the limitations improving the visible driven photoactivity and ultimate photocatalytic efficiency of titania photocatalysts [13]. In order to obtain TiO_2-based visible light activated photocatalysts, many strategies including metal ions doping [14], nonmetal ions doping [15], and coupling with other semiconductors containing narrower band gaps [16] have been adopted. Despite some controversial efficiency results obtained under different experimental conditions, introduction of transition metal cations including ferric ion (Fe^{3+}) in titania has yet been considered an effective approach towards enhancing the photocatalytic properties within the visible light region [17-19]. Being able to be replaced into TiO_2 network structure due to its electron configuration, different optimum amounts of Fe^{3+} incorporated in TiO_2 as: 0.3 wt.% [20], 0.5 wt.% [21], and 1.0 wt.% [22] have been reported in the literature.

As the leading element which has been investigated extensively in the literature due to its favorable features as a dopant, nitrogen (N) can be easily introduced in the crystal lattice of TiO_2 while suppressing the recombination rate of the photogenerated electron/hole pairs and ultimately facilitating its visible-light photocatalytic activity [23]. Park et al. [24] investigated the enhanced visible driven photocatalytic degradation of methylene orange (MO) N-doped TiO_2 nanocomposite fabricated by using graft polymerization. In another research, Bergamonti and colleagues [25] reported the synthesis of N-TiO_2 photocatalysts employing a variety of precursors as oxysulfate (N-TiA), tetraisopropoxide (N-TiU), and titanium (IV) for MO and rhodamine B (RhB) photodegradation. Based on the results obtained, N-TiA led to the highest photocatalytic activity owing to its capacity absorb higher wavelengths of light in the UV-visible spectrum. Meanwhile, suggesting greater surface area, higher capacities for adsorbing pollutant molecules, and higher photoactivity while being bond-conjugated to TiO_2, SiO_2 has also become a potential candidate in order to obtain enhanced photodegradation efficiencies in the last decades [26]. Chun and coworkers [27-29] thoroughly investigated the adsorption and photodegradation of various dyes using the SiO_2/TiO_2 photocatalyst, shedding light on its high potential.

The present study attempts to compare visible driven photocatalytic degradation of OTC by unsupported TiO_2 nanoparticles and with TiO_2 nanocomposites modified by doping a metal (Fe^{3+}), nonmetal (N), and coupling an oxide semi-conductor compound (SiO_2) in order to have a better understanding of the advantages these modifications can bring along. The experiments successfully resulted in the fabrication of the modified Fe-N-SiO_2/TiO_2 photocatalyst. Following the physicochemical and optical characterization of the as-obtained photocatalysts, As the main objective of the research, effects of four factors including catalyst loading (0.5-1.5 g/l), OTC concentration (50- 200 mg/l), initial pH (3-11), and irradiation time (0.5-6.5 h) were thoroughly investigated.

2. MATERIAL AND METHODS

2. 1. Materials Oxytetracycline (OTC) pure powder ≥ 99.9% was ordered from Sigma, USA. Tetra n-butylorthotitanate (TNBOT) ≥ 98%, Tetraethyl Ortho Silicate (TEOS) ≥ 98%, Ethanol 96%, HCl 37%, NH_3 as the nitrogen source, and $Fe(NO_3)_3.9H_2O$ as Fe^{+3} source were all supplied from Merck, Germany. All the other reagents used were all analytical grade without further requirement for purification. All aqueous solutions were prepared with ultra-pure water.

2. 2. Synthesis OF Fe-N-SiO_2/TiO_2 Catalysis Fe-N-SiO_2/TiO_2 photocatalyst was synthesized via the sol-gel technique [21]. 25 ml of TNBOT was dissolved in 100 ml of ethanol under magnetic stirring for 30 min (A solution). Then, 1.6 ml of ethanol was added to TEOS under stirring for 10 min followed by the addition of 4 ml of HCl 37% + 3 ml of ultra-pure water and then further stirred for 30 min (B solution). Next, C solution was prepared by dissolving 0.148 g of $Fe(NO_3)_3.9H_2O$ in 20 ml of ethanol under stirring for 10 min. Ultimately, the mixture of NH_3, and B and C solutions were added to A solution followed by being stirred for about 6 h. The final solution was aged for 48 h. The prepared sample was then dried at 100 ^oC for approximately 10 h, ultimately being calcinated at 450 ^oC for 2.5 h.

2. 3. Characterization of the Prepared Photacatalysts Using KBr pellets containing the powder samples, an FT-IR spectrometer (MAGNA-560) was applied to record Fourier Transform Infra-Red (FT-IR) spectra. X-ray diffractometer (a Rigaku D-max C III) with Ni-filtered Kα radiation and Philips XL30 microscope with accelerating voltage of 10 kV made it possible to obtain X-ray diffraction (XRD) patterns and scanning electron microscopy (SEM) images, respectively leading to a better observation and estimation of the photocatalysts morphology and their structural properties. UV-Vis spectrophotometer (Rayleigh UV 2601 model) and the photoluminescence spectrometer using a photomultiplier tube (Perkin Elmer LS55) were used to study DRS and PL analysis, respectively.

2. 4. Photodegradation Experiments Photodegradation performance of the synthesized photocatalysts was evaluated by degrading the synthetic OTC wastewater. Reaction suspensions were prepared by adding appropriate amounts of the as-prepared photocatalyst powders into 200 ml of the synthetic OTC wastewater. Solutions were then irradiated by ultraviolet (UV) and visible (Vis) lights for specific time intervals. Experiments were performed for 390 min, and liquid aliquots (5 ml) were withdrawn every 60 min. The samples were then centrifuged to remove the existing particles prior to being analyzed by UV-Vis spectrophotometry. COD concentration of the samples were measured using standard method (5220D) procedures [30]. In each sample, OTC concentration was measured according to its absorbance detected by a UV–Vis spectrophotometer (DR 5000, Jenway) at maximum wavelength of 348 nm. In order to better compare the results, bare Titania was also tested along with the other samples under the same experimental conditions.

2. 5. Experimental Set Up As shown in Figure 1, the photodegradation tests in the laboratory scale were conducted in a suspended batch photoreactor. Being located in a black box, the photoreactor consisted of a 200 ml Pyrex-glass cell. Irradiation sources were a 100-watt tungsten lamp and a UV lamp (HITACHI, emission: 365 nm, constant intensity 60 mW/cm^2) which were located at the upper part of the photoreactor. The vertical distance between the solution and the irradiation source was 15 cm. Furthermore, a magnetic stirrer was applied to keep the solution uniformed by providing constant agitation throughout the experiments at the constant temperature of 25±1 °C.

2. 6. Experimental Design As one of the most common experimental methods, response surface methodology (RSM) under Design Expert software (Stat-Ease Inc., version 11.1.2.0) was employed to design the photodegradation tests as well as their mathematical modeling leading to further data analysis [31]. Accordingly, four independent numerical factors including initial OTC concentration, catalyst concentration, reaction time, and initial pH were assessed in terms of their effects on the OTC removal process performance and modeled at 5 levels (α=±0.5) by inscribed central composite design (CCID) as shown in Table 1. According to the following equation, a total of 30 operating conditions [32] (Equation (1)) were designed.

$$N = 2^{k-q} + 2\times k + n_c \quad (1)$$

where k, q, and n_c are considered as the number of factors, a fraction of the number factor (which is zero for full factorial design) and the replicate number of the central point, respectively [32]. The values of the responses obtained in the experiments are presented in Table 2.

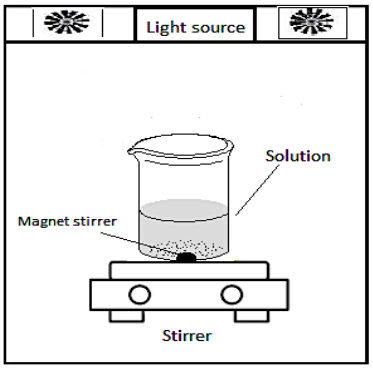

Figure 1. The schematic of the employed photocatalytic batch reactor

TABLE 1. Expermental range and levels of the independed variables

Variables	Range and levels				
	-1	-α	0	+α	1
A- Initial OTC concentration, mg/l)	50	87.5	125	162.5	200
B-Catalyst concentration, g/l	0.5	0.75	1	1.25	1.5
C- Initial pH	3	5	7	9	11
D- Reaction time, h	0.5	2	3.5	5	6.5

3. RESULTS AND DISCUSSION

3. 1. Photocatalytic Activity Experiments: Optimization of Fe-N-SiO_2/TiO_2 Each prepared photocatalyst was subjected to a photocatalytic reaction for OTC removal at certain conditions (OTC concentration = 50 ppm and photocatalyst concentration = 0.5g/l) under visible light for 6.5 h (390 min). The prepared samples included pure TiO_2 and its combination with different mass ratios of the dopants (Fe-TiO_2, N-TiO_2, SiO_2-TiO_2, and Fe-N-SiO_2-TiO_2). As observed in Figure 2, pure TiO_2 did not exhibit much visible photoactivity (only 40%). The optimum weight fractions of Fe, N, and SiO_2 as the dopants were obtained at 0.05, 5, and 5 wt. %, respectively, and were further applied in the modified photocatalysts.

Undergoing the same visible light irradiation for 390 min, all of the doped nanocomposites led to higher visible light activities in comparison to the pure TiO_2 as shown in Figure 2. Fe-N-SiO_2/TiO_2, resulting in 91 % OTC removal efficiency, showed the maximum visible-light photocatalytic activity compared to the other doped photocatalysts: Fe-TiO_2 (80%) N-TiO_2 (70%), SiO_2-TiO_2 (64%).

TABLE 2. Experimental conditions for the photocatalytic process

Run	Factor 1	Factor 2	Factor 3	Factor 4	Response 1	Response 2
	A: OTC concentration	B: Catalyst concentration	C: Initial pH	D: Reaction time	OTC removal eff.	SRR
	mg/l	g/l		h	%	mg $_{OTC\ removed}$/ g $_{cat}$. h
1	50	0.5	3	6.5	80.26	12.34
2	50	0.5	3	0.5	56.36	78.35
3	50	0.5	11	0.5	25.26	31.86
4	50	0.5	11	6.5	45.93	7.06
5	50	1.5	3	6.5	86.93	4.45
6	50	1.5	11	0.5	22.09	8.1
7	50	1.5	11	6.5	62.26	3.19
8	50	1.5	3	0.5	60.26	24.2
9	87.5	1	7	3.5	92.1	20.5
10	125	0.75	7	3.5	71.09	29.75
11	125	1	7	3.5	73.35	23.1
12	125	1	7	3.5	75.9	25.28
13	125	1	7	5	83.84	19.01
14	125	1	9	3.5	75	23.561
15	125	1	7	3.5	75.1	25.21
16	125	1	7	3.5	73.4	25.99
17	125	1	7	2	70.9	35.45
18	125	1	7	3.5	73.1	23.2
19	125	1	7	3.5	73.9	25.8
20	125	1	5	3.5	84.5	26.5
21	125	1.25	7	3.5	83.3	20.1
22	162.5	1	7	3.5	78.2	32.04
23	200	0.5	3	0.5	33.5	173
24	200	0.5	11	6.5	31.56	19.42
25	200	0.5	11	0.5	23	119.73
26	200	0.5	3	6.5	53.56	32.96
27	200	1.5	3	6.5	83.98	51.68
28	200	1.5	11	6.5	42.9	8.8
29	200	1.5	3	0.5	70.45	347.2
30	200	1.5	11	0.5	28.3	51.7

The improved visible driven photocatalytic activity of Fe-doped TiO_2 (80%) is attributed to the narrower band gap leading to the enhanced generation of the charge carriers and higher photocatalytic activity [17, 33, 34]. Furthermore, acting as shallow traps in the titania lattice, Fe^{3+} cations lead to a reduction in electron-hole recombination properties, hence increasing not only the electron-hole pair lifetime but also the possibility of reactions between the created electron-hole pair. As for N-doped TiO_2, owing to the formation of a mid-gap (N ^{2}p) with an intermediate energy level over top of the (O ^{2}p) valence band [35], introducing nitrogen into the TiO_2 lattice results in its narrower band gap and ultimately enhanced its photocatalytic activity under visible light irradiation. While in SiO_2-TiO_2 composite, the semi-conductor cations entering the lattice of TiO_2 not only provides more available surface for photocatalytic activity, but also enhances its surface acidity. Consequently, coupling SiO_2 with TiO_2 leads to preferentially adsorbing more hydroxyl groups on the surface of the composite and therefore, decreasing its contamination by OTC [36].

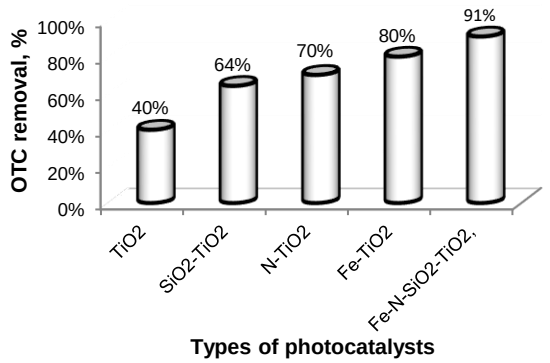

Figure 2. Visible-driven OTC removal efficiency by different photocatalysts at the OTC concentration of 50 ppm and photocatalyst concentration of 0.5g/l for 390 min

Relying on the aforementioned reasons supporting the improved visible driven photocatalytic activity in three modified nanocomposites, Fe-N-SiO_2/TiO_2 obtained the highest OTC removal efficiency, simultaneously benefiting from the addition of Fe^{3+}, N, and SiO_2.

3. 2. Characterization of Fe-N-Sio₂/Tio₂ Photocatalyst

3. 2. 1. FT-IR Spectroscopy Figure 3 illustrates the FT-IR spectra of the prepared samples. The bands at 400-800 are related to the vibration of Ti-O and Ti-O-Ti bonds in all of the samples [30]. The presence of dissolved or atmospheric CO_2 in the samples also resulted in a peak at 2400 cm^{-1}. Furthermore, the weak transmittance bands at around 1630 and 3100-3600 cm^{-1} can be assigned respectively to the bending and stretching vibrations of hydroxyl groups of the adsorbed water molecules in the samples [37]. Owing to the nitrogen atoms being substituted into the TiO_2 network in N-TiO_2 and Fe-N-SiO_2-TiO_2, the peak at 1440 cm^{-1} was obtained in Figure 3 [38].

The asymmetric vibration of Si–O–Si bonds for SiO_2-TiO_2 composites was observed at approximately 1060 cm^{-1} [50]. The stretching vibrations of Si–OH, SiO^- groups and Si–O–Ti bonds can be implied by the absorption band at about 900~1000 cm^{-1} [39].

3. 2. 2. XRD Patterns The XRD pattern was employed to identify crystal structure of the prepared pure TiO_2, SiO_2-TiO_2, N-TiO_2, Fe-TiO_2 and Fe-N-SiO_2-TiO_2 photocatalysts as illustrated in Figure 4. At all samples, the peaks are noted to tetragonal anatase crystalline phase of TiO_2. The diffraction peaks of the 2θ values at 25.1°, 37.25°, 38.63°, 48.12°, 54.48°, 62.54°, 68.9°, 70.57°, and 75.15° were observed which are related to the crystalline phases of anatase. The XRD pattern for the doping amount of Fe (0.05 wt. %) was too low to be detected by XRD [40]. The crystalline size (D) of Fe-N-SiO_2/TiO_2 nanoparticles was calculated by using Debye Scherrer's formula ($D = 0.9\lambda/\beta\cos\theta$), where λ is the wavelength of the X-rays and β is the full width at the half maximum intensity (FWHM) [41]. The results of the calculations for the XRD data showed that the range of particle sizes of Fe-N-SiO_2/TiO_2 NPs are between 19.64 to 46.78 nm, which is close to and supports SEM results.

3. 2. 3. SEM Analysis The SEM images of the Fe-N-SiO_2/TiO_2 nanoparticles are depicted in Figures 5(a)-5(c). As observed in Figure 5(a), the sizes of the nanoparticles were in the range of 22.14-50.87 nm. As an extra provision to calculate the size of the catalyst, Figure 5b presented the particle size distribution of Fe-N-SiO_2/TiO_2 nanoparticles in the range of 10 to 45 nm, in which the most common size range included the values from 26 to 30 nm [42]. The SEM results are the clear evidence that the uniformly distributed nanoparticles are spherical in shape. Providing more active areas for photocatalytic degradation, the porous structure of the as-prepared photocatalysts has also been proven by these images [40]. The EDX result in Figure 5(c) confirms the presence of Fe, N, Si, Ti and O elements in the nanocomposite.

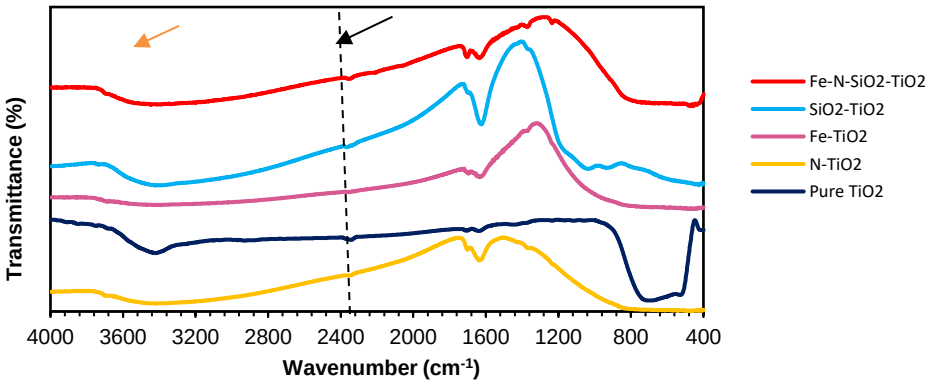

Figure 3. FT-IR spectra of the prepared samples

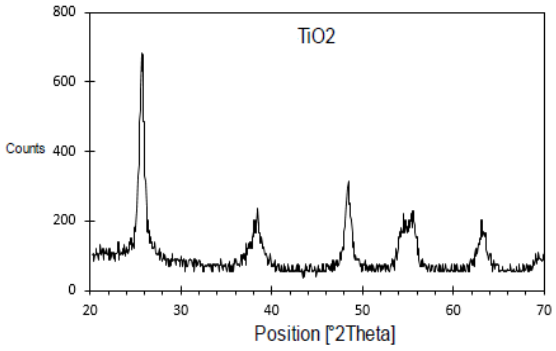

(a)

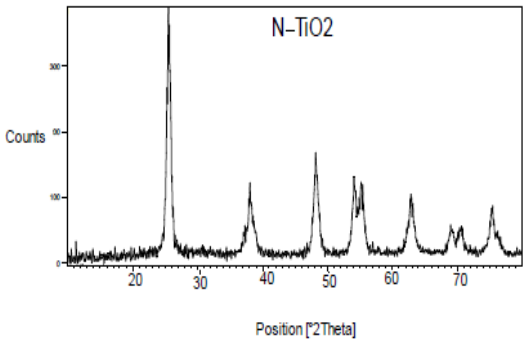

(b)

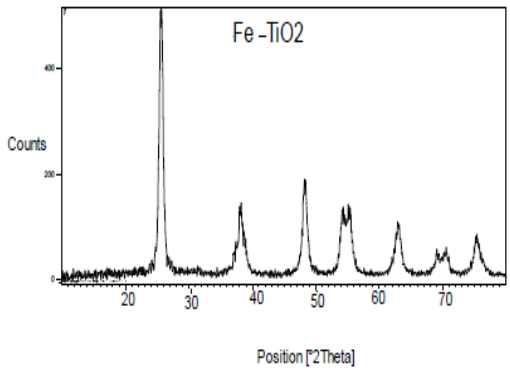

(c)

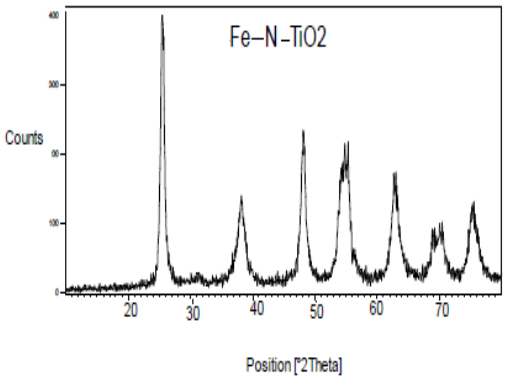

(d)

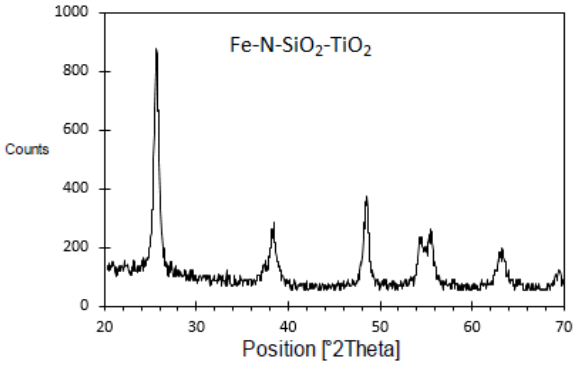

(e)

Figure 4. XRD patterns of the prepared samples

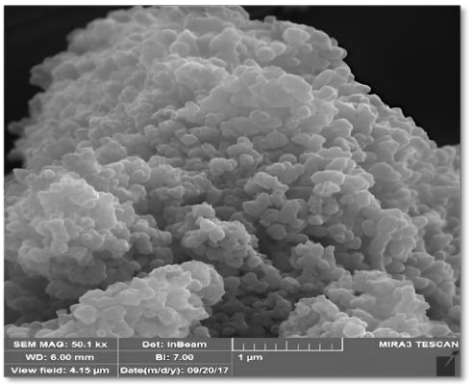

(a)

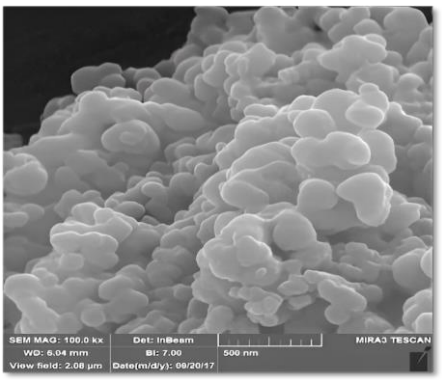

(b)

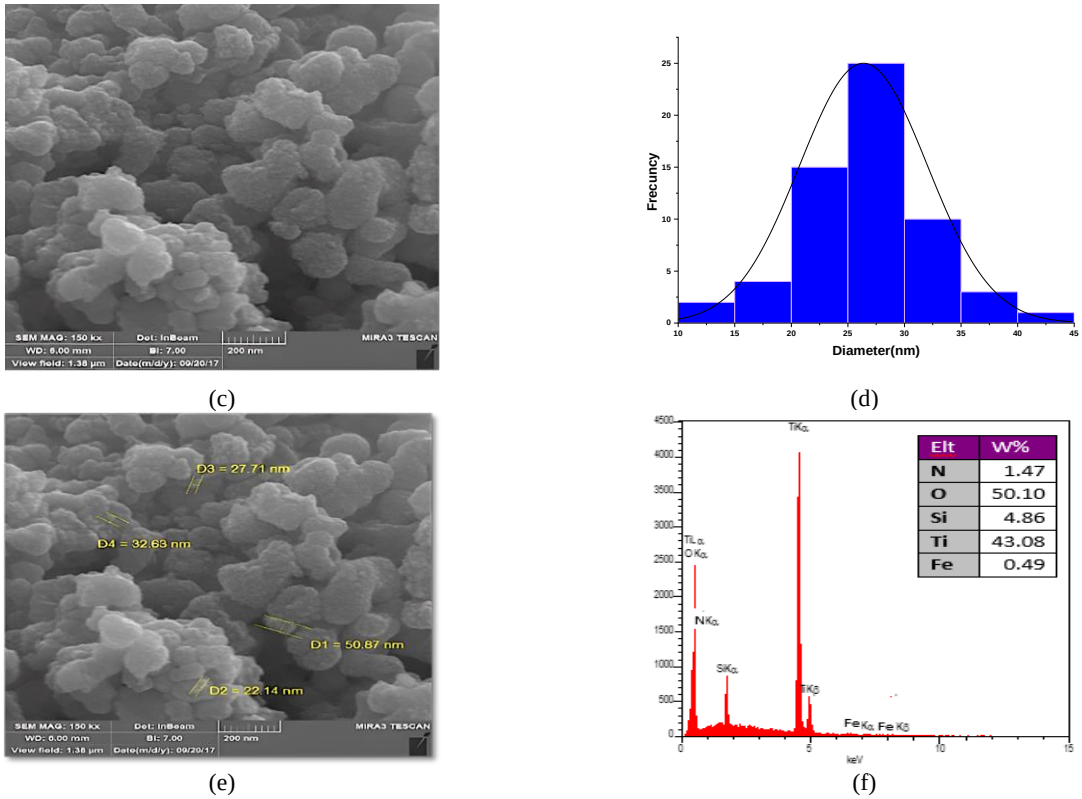

Figure 5. SEM images and EDX spectrum of Fe-N-SiO_2/TiO_2

3. 2. 4. Optical Properties The optical absorption of the synthesized photocatalyst was assessed by UV-Vis DRS analysis and its result was indicated in Figure 6(a). The strong absorption in the visible light region implies the vital role of dopant agents (Fe and N elements) in the reduction of band gap and extension of the absorption edge into a visible light range. Figure 6(b) shows the PL emission spectrum of pure TiO_2 and Fe-N-SiO_2/TiO_2 photocatalysts. The PL intensity of modified nanocomposite is lower than pure TiO_2 due to incorporating Fe, N, and SiO_2 on the TiO_2 surface [43, 44]. Both oxygen vacancies and lattice defects in the structure of the modified TiO_2 sample can act as charge carrier trapping centers and infer the recombination rate of photogenerated h+/e- pairs decline.

3. 3. Photodegradation Process Analysis And Modeling In order to fit the CCID experimental results obtained in OTC photodegradation runs, a response surface model using standard analysis of variance (ANOVA) was developed and the subsequent results are provided in Table 3. Two models, reduced quadratic and reduced 2FI, containing the confidence level of 99 % (probability value <0.0001) were selected for the OTC removal efficiency and specific removal rate (SRR), respectively.

Implying the degree of significance and influence of the coefficients on the responses, the probability values (p-values) and F-values are given in Tables 3 and 4. The insignificant model terms with significantly higher than 0.05 p-values need to be removed from the model equation simplifying the model. As a result, according to p-values for OTC removal, the significant model terms include A (OTC concentration), B (catalyst concentration), C (initial pH), D (reaction time), AB, AD, BC, and B^2. Meanwhile, for SRR, A, B, C, D, AB, AC, and BC are considered significant model terms. Given the F-values and also multilateral contributions of each variable in the final equation, significant model terms were indicated in terms of their order and subsequent influences on both responses.

Evaluating the accuracy and variability of the model for the OTC removal efficiency and SRR, the high values of the coefficient of determination (R^2 = 0.9487 and R^2 = 0.9570, respectively) ensures a satisfactory adjustment of the developed models to the experimental data [45]. Furthermore, being very close to the corresponding R^2 value, the adjusted R^2 values of respectively 0.9291 and 0.9458 further confirm the adaptability of the aforementioned models. Predicted R^2 values of both responses are in good agreement with experimental values (Predicted R^2 was about 0.8721 and 0.8900 for OTC removal and SRR, respectively).

According to Table 3, the adequate precision values for OTC removal efficiency and SRR were 23.8605 and 44.2257, respectively, further proving that the models are desirable. Figures 7(a) and 7(b) depict the measured data versus the predicted ones for both models. Furthermore, coefficient of variation (C.V. %) is an important concept allowing us to predict variables within and outside data sets [45]. High reliability and accuracy of experimental work in this study could also be explained by C.V. values of 9.07% and 6.99% for OTC removal and SRR, respectively.

Favoring more effective contacts between the OTC and hydroxyl radicals, the conceivable effect of longer reaction time on the response was observed in both plots.

The three-dimensional (3D) response surface plots represented in Figures. 8 and 9 are applied to assess the interaction effects of the aforementioned variables on both responses. The concentration of OTC was held constant at an average level (125 mg/l) in all of the plots given in Figure 8. In the meantime, increasing the OTC concentration to the maximum level might have an inhibiting role due to the saturation of the photocatalyst active sites with OTC molecules. As a result, the poisoning phenomenon might occur at high OTC loadings, resulting in less production of hydroxyl radicals and superoxide radical anions thereby weakening the degradation efficiency [46].

TABLE 3. ANOVA results for the selected models regarding OTC removal efficiency.

Source	Sum of Squares	df	Mean Square	F-value	p-value		
Model	12684.80	8	1585.60	48.53	< 0.0001	Significant	**Final Equation in Terms of Coded Factors**
A-OTC conc.	378.72	1	378.72	11.59	0.0027		
B-Cat. conc.	785.50	1	785.50	24.04	< 0.0001		
C-Initial pH	3750.09	1	3750.09	114.78	< 0.0001		OTC removal eff. =
D-Reaction time	1848.22	1	1848.22	56.57	< 0.0001		+78.18
AB	227.10	1	227.10	6.95	0.0154		-4.79 A
AD	186.73	1	186.73	5.72	0.0263		+6.90 B
BC	144.84	1	144.84	4.43	0.0475		-15.08 C
B^2	5363.59	1	5363.59	164.17	< 0.0001		+10.58 D
Residual	686.09	21	32.67				+3.77 AB
Lack of Fit	679.76	16	42.48	33.57	0.0005	Significant	-3.42 AD
Pure Error	6.33	5	1.27				-3.01 BC
Cor Total	13370.89	29					-27.58 B^2

Fit Statistics

Std. Dev	Mean	C.V. %	R^2	Adjusted R^2	Predicted R^2	Adeq Precision
5.72	63.01	9.07	0.9487	0.9291	0.8721	23.8605

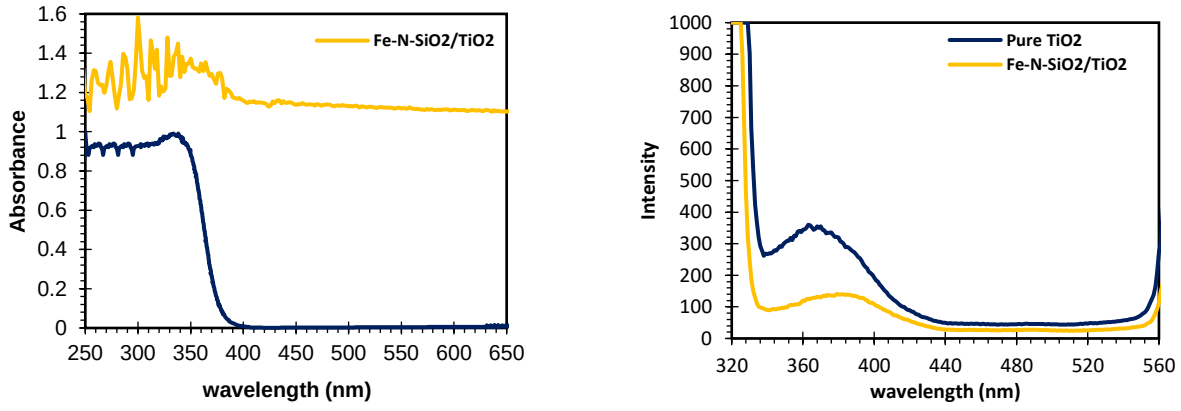

(a) (b)

Figure 6. (a) DRS and (b) PL spectra of the prepared photocatalysts

Figures 8(a) and 8(b) demonstrate the influence of B (catalyst concentration) and C (initial pH) on OTC removal efficiency. Being highly influenced by the initial pH of the solution in terms of its photolytic and hydrolytic stability in deionized water while presenting pKa values of 3.22, 7.46, and 8.94, OTC shows repulsive or attractive interactions with the amphoteric nature of the TiO_2-based photocatalyst in different pH levels. Thus, pH is expected to play a key role in OTC photocatalytic degradation experiments. As such, Figures 8(a) and 8(b) show that at an average OTC concentration of 125 mg/l, as initial pH level goes from acidic to basic (3 to 11), OTC removal efficiency decreases, proving the detrimental effect of basic pH levels to OTC mineralization. The observed decreasing trend can be attributed to the presence of negatively charged OTC molecules at high pH (9 and above), with a high electrical density on the ring system, which tend to attract increasing concentration of reactive species such as an hydroxyl radicals, thus affecting OTC mineralization [47]. The low degree of OTC mineralization implies that consumed OTC mainly transforms to byproducts.

However, it is noted that progressive increase in the catalyst loading from 1 to 1.5 g/l led to a decreasing trend in the response. As observed, at higher than 1g/l catalyst loadings, turbidity increases leading to the unfavorable light scattering phenomenon, and thus, the reduction of light penetration into the suspension [48]. Consequently, the decreased photoactivated volume of the suspension resulted in lower OTC removal efficiencies.

TABLE 4. ANOVA results for the selected models regarding SRR

Source	Sum of Squares	df	Mean Square	F-value	p-value		
Model	5.04	7	0.7194	82.82	< 0.0001	Significant	
A-OTC conc.	1.73	1	1.73	199.64	< 0.0001		**Final Equation in Terms of Coded Factors**
B-Cat. conc.	0.2903	1	0.2903	33.42	< 0.0001		
C-Initial pH	0.6458	1	0.6458	74.34	< 0.0001		
D-Reaction time	2.07	1	2.07	237.85	< 0.0001		
AB	0.1769	1	0.1769	20.36	0.0002		
AC	0.0335	1	0.0335	3.86	0.0623		
BC	0.0889	1	0.0889	10.24	0.0041		$Log_{10}(SRR)$= +1.41 + 0.3242A - 0.1326B - 0.1978C - 0.3539D + 0.1051AB - 0.0746BC
Residual	0.1911	22	0.0087				
Lack of Fit	0.1885	17	0.0111	21.23	0.0016	Significant	
Pure Error	0.0026	5	0.0005				
Cor Total	5.23	29					

Fit Statistics

Std. Dev	Mean	C.V. %	R^2	Adjusted R^2	Predicted R^2	Adeq Precision
0.0988	1.41	6.99	0.9570	0.9458	0.8900	44.2257

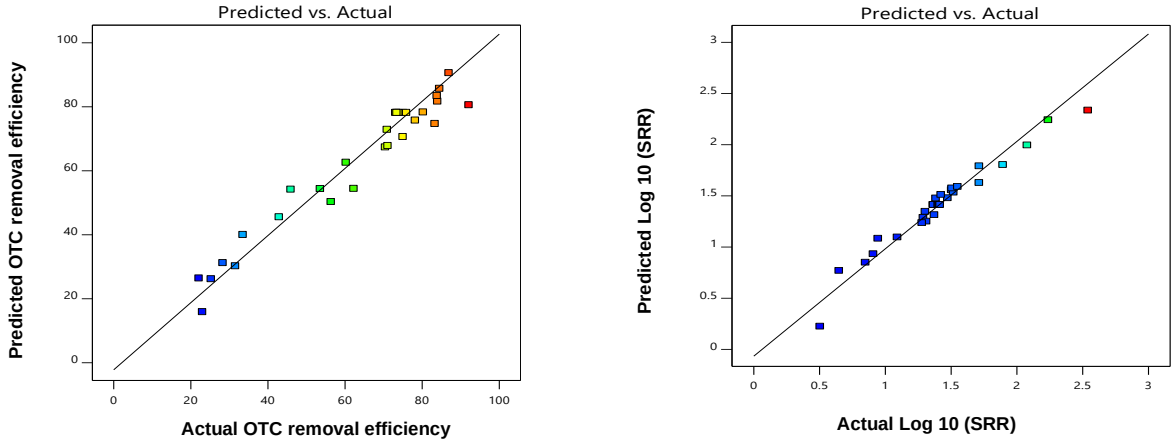

(a) (b)

Figure 7. Predicted vs. actual values plot for (a) OTC removal efficiency and (b) SRR

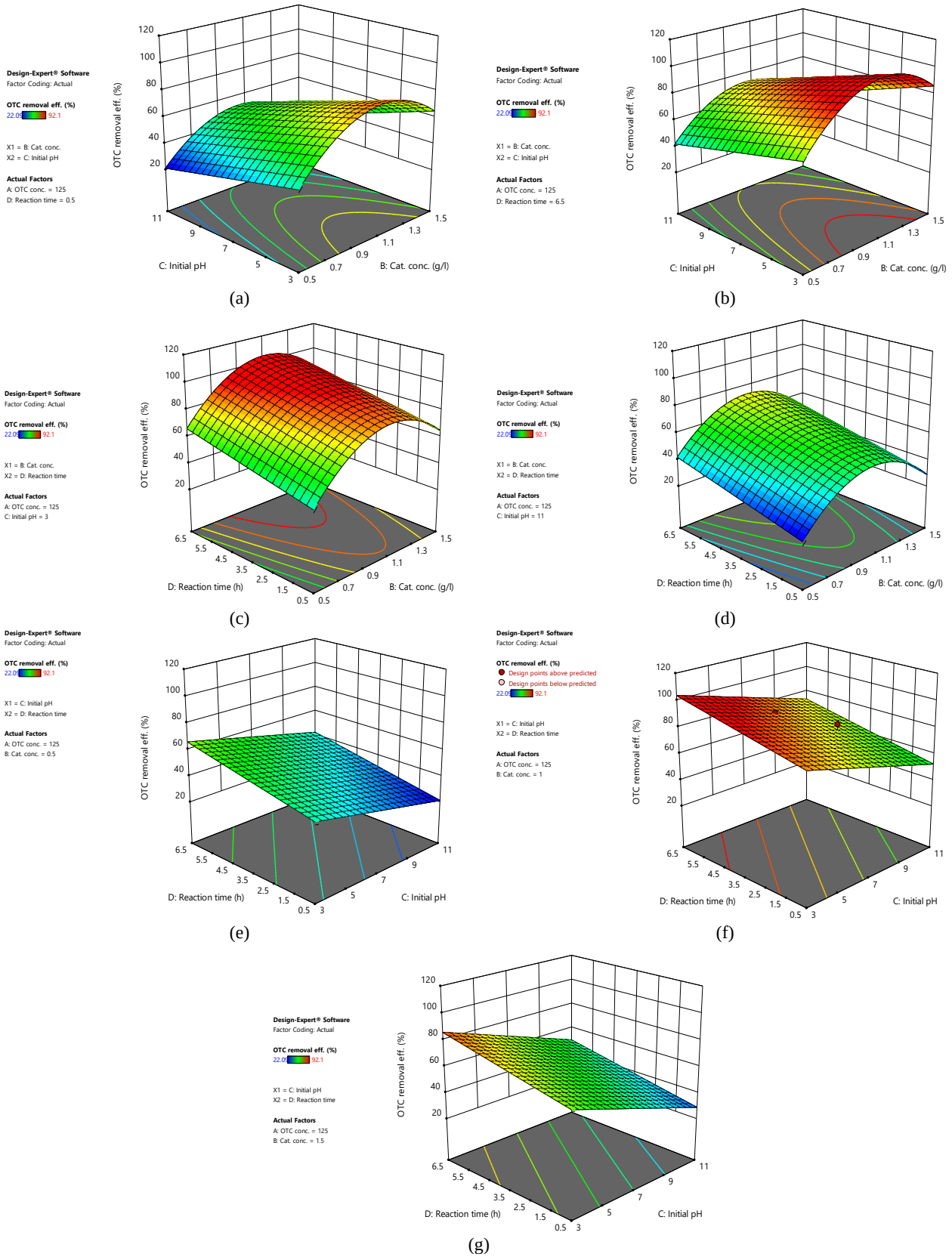

Figure 8. 3D surface plots of OTC removal for the most important pairs of factors: a and b) catalyst concentration and initial pH, c and d) catalyst concentration and reaction time, e, f and g) initial pH and reaction time

As indicated from both plots, the reaction time presented a linear positive effect on the response from 0.5 to 6.5 h. The influence of B (catalyst concentration) and D (reaction time) on the response is plotted in Figures 8(c) and 8(d). The aforementioned impact of catalyst loading on the response is represented again in these two plots, further proving the two consecutive ascending and descending trends observed below and above 1 g/l of catalyst loadings, respectively.

Favoring more effective contacts between the OTC and hydroxyl radicals, the conceivable effect of longer reaction time on the response was observed in both plots. Similarly, initial pH, showed a linear increasing impact on the response at the constant concentration of 125 mg/l of OTC.

Figures 8(e), 8(f), and 8(g) display the 3D surface plots of the response as a function of C (initial pH) and D (reaction time) at three different levels of catalyst concentration (0.5, 1, and 1.5 g/l) and average OTC concentration (125 mg/l). These plots further confirm the linear positive impacts of both initial pH and reaction time on the OTC removal efficiency. Meanwhile, the catalyst loading depicted a parabolic trend opening downward. It means that it has an increasing impact on removal efficiency until reaching catalyst concentration of 1 g/l and then reversing its impact from 1 to 1.5 g/l. In order to assess the overall photocatalytic performance, treatment capacity, and mass efficiency of the prepared photocatalyst, specific OTC removal rate (SRR) was plotted as a function of different variables in Figures 9(a)-9g. The reaction time remained at the minimum level of 0.5 h. It is clear that reaction time has a decreasing impact on the SRR, referring to the possible surface poisoning of the catalyst. Figure 8 (a, b, and c) represents the response surface plots for the SRR as a function of A (OTC concentration) and B (catalyst concentration) at the minimum reaction time (0.5 h) and different initial pH levels (3, 7, and 11). As observed in these plots, initial pH has a decreasing impact on SRR owing to the repulsive interaction between the catalyst surface and contaminant at higher pH levels. Furthermore, Figures 9d and 9(e) represent the effects of A (OTC concentration) and C (initial pH) at constant minimum reaction time (0.5 h) and minimum and maximum levels of catalyst loading, further highlighting the impacts of catalyst loading and initial pH on this response. The 3D plots given in Figures 9(f) and 9(g) indicate the effects of B (catalyst concentration) and C (initial pH) at the minimum reaction time (0.5 h) and minimum and maximum OTC concentrations (50 and 200 mg/l, respectively). It is noted that at higher OTC concentrations and acidic pH of 3, catalyst loading shows an increasing trend, further confirming the enhanced mass efficiency of the photocatalyst in this condition. According to the plots shown in Figures 9(a), 9(e), and 9(g), maximum SRR of

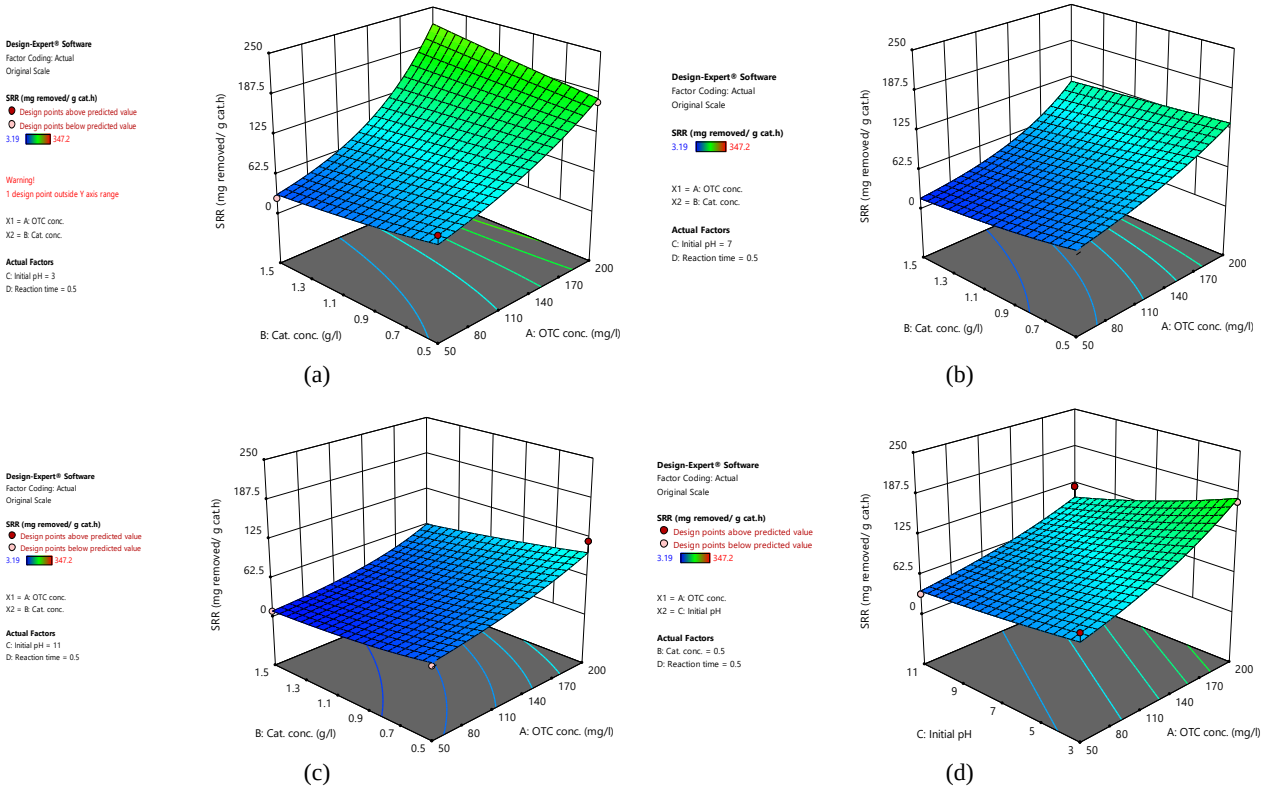

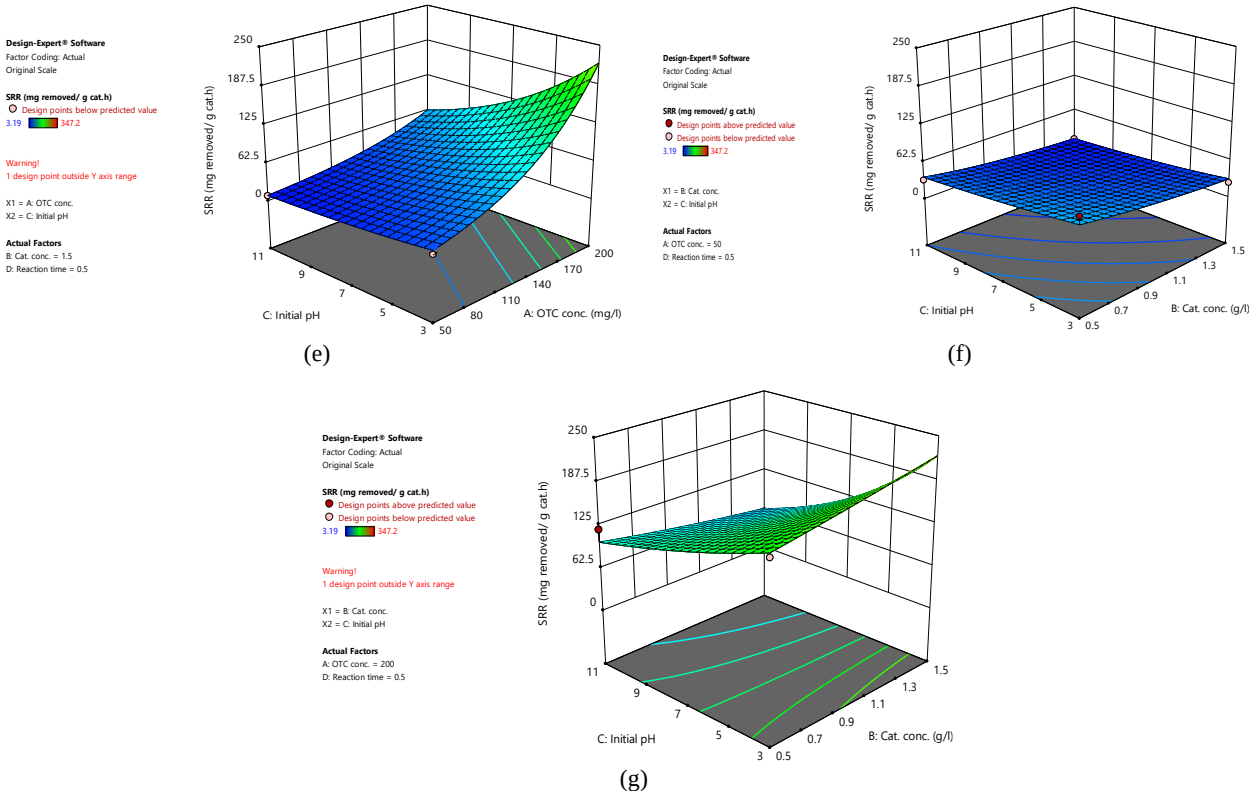

Figure 9. 3D surface plots of OTC removal for the most important pairs of factors: a, b, and c) catalyst concentration and OTC concentration, d and e) OTC concentration and initial pH, f and g) catalyst concentration and initial pH

approximately 220 mg $_{\text{OTC removed}}$/g $_{\text{cat}}$. h was obtained at initial pH of 3, minimum reaction time of 0.5 h, maximum catalyst loading of 1.5 g/l, and maximum OTC concentration of 200 mg/l.

3. 4. Photolytic Degradation of OTC under Controlled pH A visible photolytic degradation experiment was carried out at the variation of pH values to monitor the OTC removal and mineralization without the addition of the photocatalyst. The results obtained after 6.5 h are given in Figure 9. As can be seen in Figure 10, after 390 min of visible light irradiation, only the range containing a minimum level of 3% to a maximum level of 22% of the initial OTC concentration was degraded at pH levels of 3 to 11 (3, 4.4, 5, 7, 9, and 11), respectively. As aforementioned in the previous part (Figures 8(a) and 8(b) analysis), as pH increases to 9 and above, the negatively charged OTC molecules tend to facilitate the photolytic degradation of OTC and, thus, the formation of more recalcitrant intermediates to mineralization, proving that photocatalysis plays a smaller role at such higher pH levels [47].

Overall, the negligible degree of OTC photolytic mineralization is enough proof of merely sufficient degradation of OTC molecules into more stable intermediates in comparison to their photocatalytic degradation [47]. Furthermore, in order to assess the contribution of dark adsorption in OTC removal efficiency, the same experiments were carried out in darkness resulting in a minimum 1% to maximum 17% at pH values of 3 to 11 respectively.

3. 5. Reusability of the Fe-N-SiO_2-TiO_2 Photocatalyst As shown in Figure 11, the reusability of the prepared modified photocatalyst used in the reactions was investigated by the degradation of OTC after 3 cycles under the same conditions. The used photocatalyst after each cycle was regenerated with 60-min aeration under visible light. As can be seen from the results, the photocatalyst could be reused without a significant loss in its activity after 3 successive runs and only an approximate reduction of 2-4% in the process performance was observed. The aforementioned loss might be caused by gradual poisoning and insignificant catalyst loss during supernatant removal after each cycle. Overall, the reusability results indicated the sufficient stability and reliability of the Fe-N-SiO_2/TiO_2 nanocomposite proving its potential for practical application.

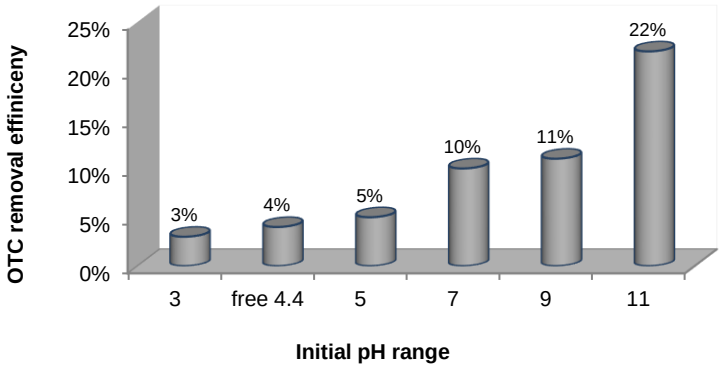

Figure 10. Photolytic degradation of OTC at different pH values (3-11) in the absence of Fe-N-SiO_2/TiO_2 under visible light irradiation for 390 min

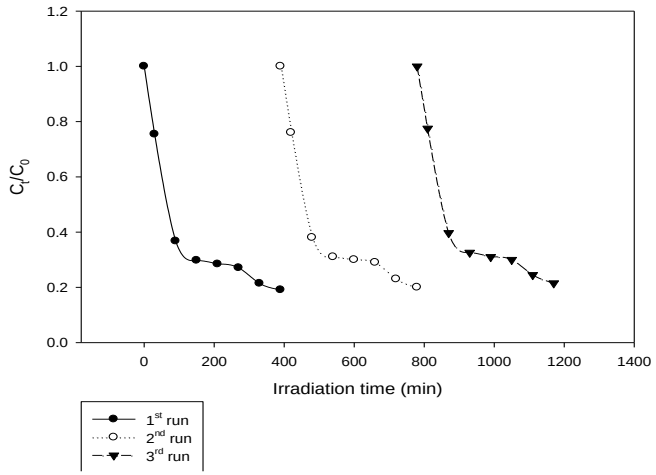

Figure 11. Reusability test of the Fe-N-SiO_2-TiO_2 photocatalyst degrading OTC during three successive runs after regular periodic regeneration using 60-min aeration under visible light

4. CONCLUSION

In the present study, in order to obtain the enhanced photocatalytic decomposition of the nonbiodegradable OTC compounds under visible light, the Fe-N-SiO_2/TiO_2 photocatalyst was successfully synthesized by sol-gel technique and its physical properties were characterized via FT-IR and SEM. The effects of OTC concentration, catalyst concentration, initial pH, and reaction time on the OTC removal efficiency and its SRR were evaluated using CCID under RSM. The reaction time had a positive effect on the OTC removal efficiency while a reverse impact was observed for the initial pH. As for the assessment of the optimum overall performance of the prepared photocatalyst, maximum SRR of 220 mg $_{OTC\ removed}$/g $_{cat}$. H at certain conditions (OTC Conc. = 200 mg/l, catalyst conc. = 1.5 g/l, pH = 3, and reaction time = 0.5 h) was obtained. Furthermore, the Fe-N-SiO_2/TiO_2 nanocomposite could easily be recovered and reused after 3 cycles without considerable loss in its photocatalytic activity.

5. ACKNOWLEDGEMENT

The authors would like to acknowledged Razi University for the financial support of present work to be accomplished and provided necessary facilities.

6. REFERENCES

1. Patel, M., Kumar, R., Kishor, K., Mlsna, T., Pittman Jr, C.U. and Mohan, D., "Pharmaceuticals of emerging concern in aquatic systems: Chemistry, occurrence, effects, and removal methods", ***Chemical Reviews***, Vol. 119, No. 6, (2019), 3510-3673. doi: 10.1021/acs.chemrev.8b00299.

2. Wang, P. and Yuan, Q., "Photocatalytic degradation of tetracyclines in liquid digestate: Optimization, kinetics and correlation studies", ***Chemical Engineering Journal***, Vol. 410, (2021), 128327. doi: 10.1016/j.cej.2020.128327.
3. Wei, Z., Liu, J. and Shangguan, W., "A review on photocatalysis in antibiotic wastewater: Pollutant degradation and hydrogen production", ***Chinese Journal of Catalysis***, Vol. 41, No. 10, (2020), 1440-1450. doi: 10.1016/S1872-2067(19)63448-0.
4. Roy, N., Alex, S.A., Chandrasekaran, N., Mukherjee, A. and Kannabiran, K., "A comprehensive update on antibiotics as an emerging water pollutant and their removal using nano-structured photocatalysts", ***Journal of Environmental Chemical Engineering***, Vol. 9, No. 2, (2021), 104796. doi: 10.1016/j.jece.2020.104796.
5. Zhu, T.-t., Su, Z.-x., Lai, W.-x., Zhang, Y.-b. and Liu, Y.-w., "Insights into the fate and removal of antibiotics and antibiotic resistance genes using biological wastewater treatment technology", ***Science of the Total Environment***, Vol. 776, (2021), 145906. doi: 10.1021/acs.est.9b01131.
6. Phoon, B.L., Ong, C.C., Saheed, M.S.M., Show, P.-L., Chang, J.-S., Ling, T.C., Lam, S.S. and Juan, J.C., "Conventional and emerging technologies for removal of antibiotics from wastewater", ***Journal of Hazardous Materials***, Vol. 400, (2020), 122961. doi: 10.1016/j.jhazmat.2020.122961 .
7. Baaloudj, O., Assadi, I., Nasrallah, N., El Jery, A., Khezami, L. and Assadi, A.A., "Simultaneous removal of antibiotics and inactivation of antibiotic-resistant bacteria by photocatalysis: A review", ***Journal of Water Process Engineering***, Vol. 42, (2021), 102089. doi: 10.1016/j.jwpe.2021.102089.
8. Zangeneh, H., Zinatizadeh, A., Habibi, M., Akia, M. and Isa, M.H., "Photocatalytic oxidation of organic dyes and pollutants in wastewater using different modified titanium dioxides: A comparative review", ***Journal of Industrial and Engineering Chemistry***, Vol. 26, (2015), 1-36. doi: 10.1016/j.jec.2014.10.043.
9. Sharma, M., Yadav, A., Mandal, M. and Dubey, K., " TiO_2 based photocatalysis: A valuable approach for the removal of pharmaceuticals from aquatic environment", ***International Journal of Environmental Science and Technology***, Vol., No., (2022), 1-16. doi: 10.1016/j.ijhydene.2019.07.241.
10. Pereira, J.H., Reis, A.C., Queirós, D., Nunes, O.C., Borges, M.T., Vilar, V.J. and Boaventura, R.A., "Insights into solar TiO_2-assisted photocatalytic oxidation of two antibiotics employed in aquatic animal production, oxolinic acid and oxytetracycline", ***Science of the Total Environment***, Vol. 463, (2013), 274-283. doi: 10.3390/catal11091039.
11. Jia, L., Jin, Y., Li, J., Wei, Z., Chen, M. and Ma, J., "Study on high-efficiency photocatalytic degradation of oxytetracycline based on a spiral microchannel reactor", ***Industrial & Engineering Chemistry Research***, Vol. 61, No. 1, (2021), 554-565. doi.
12. Chen, D., Cheng, Y., Zhou, N., Chen, P., Wang, Y., Li, K., Huo, S., Cheng, P., Peng, P. and Zhang, R., "Photocatalytic degradation of organic pollutants using TiO_2-based photocatalysts: A review", ***Journal of Cleaner Production***, Vol. 268, (2020), 121725. doi: 10.1016/j.jclepro.2020.121725.
13. Basavarajappa, P.S., Patil, S.B., Ganganagappa, N., Reddy, K.R., Raghu, A.V. and Reddy, C.V., "Recent progress in metal-doped TiO_2, non-metal doped/codoped TiO_2 and TiO_2 nanostructured hybrids for enhanced photocatalysis", ***International Journal of Hydrogen Energy***, Vol. 45, No. 13, (2020), 7764-7778. doi: 10.1016/j.ijhydene.2019.07.241.
14. Jiang, D., Otitoju, T.A., Ouyang, Y., Shoparwe, N.F., Wang, S., Zhang, A. and Li, S., "A review on metal ions modified TiO_2 for photocatalytic degradation of organic pollutants", ***Catalysts***, Vol. 11, No. 9, (2021), 1039. doi: 10.3390/catal11091039.
15. Akhter, P., Arshad, A., Saleem, A. and Hussain, M., "Recent development in non-metal-doped titanium dioxide photocatalysts for different dyes degradation and the study of their strategic factors: A review", ***Catalysts***, Vol. 12, No. 11, (2022), 1331. doi: 10.3390/catal12111331.
16. Del Angel, R., Durán-Álvarez, J.C. and Zanella, R., "Tio2-low band gap semiconductor heterostructures for water treatment using sunlight-driven photocatalysis", ***Titanium Dioxide: Material for a Sustainable Environment***, Vol. 305, (2018). doi: 10.5772/intechopen.76501.
17. Sood, S., Umar, A., Mehta, S.K. and Kansal, S.K., "Highly effective fe-doped TiO_2 nanoparticles photocatalysts for visible-light driven photocatalytic degradation of toxic organic compounds", ***Journal of Colloid and Interface Science***, Vol. 450, (2015), 213-223. doi: 10.1016/j.jcis.2015.03.018 .
18. Wang, J., Li, X., Ren, Y., Xia, Z., Wang, H., Jiang, W., Liu, C., Zhang, S., Li, Z. and Wu, S., "The effects of additive on properties of fe doped TiO_2 nanoparticles by modified sol-gel method", ***Journal of Alloys and Compounds***, Vol. 858, (2021), 157726. doi: 10.1016/j.jallcom.2020.157726.
19. Xia, Z., Xing, S., Wang, H., Zhao, D., Wu, S., Jiang, W., Wang, N., Liu, S., Liu, C. and Ding, W., "Weak-visible-light-driven fe doped TiO_2 photocatalyst prepared by coprecipitation method and degradation of methyl orange", ***Optical Materials***, Vol. 129, (2022), 112522. doi: 10.1016/j.optmat.2022.112522.
20. Kerkez-Kuyumcu, Ö., Kibar, E., Dayıoğlu, K., Gedik, F., Akın, A.N. and Özkara-Aydınoğlu, Ş., "A comparative study for removal of different dyes over m/ TiO_2 (M= Cu, Ni, Co, Fe, Mn and Cr) photocatalysts under visible light irradiation", ***Journal of Photochemistry and Photobiology A: Chemistry***, Vol. 311, (2015), 176-185. doi: 10.1016/j.jphotochem.2015.05.037.
21. Moradi, V., Jun, M.B., Blackburn, A. and Herring, R.A., "Significant improvement in visible light photocatalytic activity of fe doped TiO_2 using an acid treatment process", ***Applied Surface Science***, Vol. 427, (2018), 791-799. doi: 10.1177/2633366X20906164.
22. Moradi, H., Eshaghi, A., Hosseini, S.R. and Ghani, K., "Fabrication of fe-doped TiO_2 nanoparticles and investigation of photocatalytic decolorization of reactive red 198 under visible light irradiation", ***Ultrasonics Sonochemistry***, Vol. 32, (2016), 314-319. doi: 10.1016/j.ultsonch.2016.03.025.
23. Chung, K.-H., Kim, B.-J., Park, Y.-K., Kim, S.-C. and Jung, S.-C., "Photocatalytic properties of amorphous n-doped TiO_2 photocatalyst under visible light irradiation", ***Catalysts***, Vol. 11, No. 8, (2021), 1010. doi: 10.3390/catal11081010.
24. Park, J.T., Kim, D.J. and Kim, J.H., "A facile graft polymerization approach to n-doped TiO_2 heterostructures with enhanced visible-light photocatalytic activity", ***Materials Letters***, Vol. 202, (2017), 66-69. doi: 10.1016/j.matlet.2017.05.070.
25. Bergamonti, L., Predieri, G., Paz, Y., Fornasini, L., Lottici, P. and Bondioli, F., "Enhanced self-cleaning properties of n-doped TiO_2 coating for cultural heritage", ***Microchemical Journal***, Vol. 133, (2017), 1-12. doi: 10.1016/j.microc.2017.03.003.
26. Joseph, C.G., Taufiq-Yap, Y.H., Musta, B., Sarjadi, M.S. and Elilarasi, L., "Application of plasmonic metal nanoparticles in TiO_2- SiO_2 composite as an efficient solar-activated photocatalyst: A review paper", ***Frontiers in Chemistry***, Vol. 8, (2021), 568063. doi: 10.3389/fchem.2020.568063.
27. Chun, H., Yizhong, W. and Hongxiao, T., "Influence of adsorption on the photodegradation of various dyes using surface bond-conjugated TiO_2/ SiO_2 photocatalyst", ***Applied Catalysis B: Environmental***, Vol. 35, No. 2, (2001), 95-105. doi: 10.1016/S0926-3373(01)00236-3.
28. Chun, H., Yizhong, W. and Hongxiao, T., "Preparation and characterization of surface bond-conjugated TiO_2/ SiO_2 and photocatalysis for azo dyes", ***Applied Catalysis B:***

Environmental, Vol. 30, No. 3-4, (2001), 277-285. doi: 10.1016/S0926-3373(00)00237-X.

29. Chun, H., Yuchao, T. and Hongxiao, T., "Characterization and photocatalytic activity of transition-metal-supported surface bond-conjugated TiO_2/SiO_2", ***Catalysis Today***, Vol. 90, No. 3-4, (2004), 325-330. doi.
30. Zangeneh, H., Zinatizadeh, A.A., Zinadini, S., Feyzi, M., Rafiee, E. and Bahnemann, D.W., "A novel l-histidine (c, n) codoped-TiO_2-CDS nanocomposite for efficient visible photo-degradation of recalcitrant compounds from wastewater", ***Journal of Hazardous Materials***, Vol. 369, (2019), 384-397. doi: 10.1016/j.jhazmat.2019.02.049.
31. Zulfiqar, M., Samsudin, M.F.R. and Sufian, S., "Modelling and optimization of photocatalytic degradation of phenol via TiO_2 nanoparticles: An insight into response surface methodology and artificial neural network", ***Journal of Photochemistry and Photobiology A: Chemistry***, Vol. 384, (2019), 112039. doi: 10.1016/j.jphotochem.2019.112039.
32. Khuri, A.I. and Cornell, J.A., "Response surfaces: Designs and analyses: Revised and expanded, CRC press, (2018). doi: 10.1201/9780203740774
33. Larumbe, S., Monge, M. and Gómez-Polo, C., "Comparative study of (n, fe) doped TiO_2 photocatalysts", ***Applied Surface Science***, Vol. 327, (2015), 490-497. doi: 10.1016/j.apsusc.2014.11.137.
34. Moradi, V., Ahmed, F., Jun, M.B., Blackburn, A. and Herring, R.A., "Acid-treated fe-doped TiO_2 as a high performance photocatalyst used for degradation of phenol under visible light irradiation", ***Journal of Environmental Sciences***, Vol. 83, No., (2019), 183-194. doi: 10.1016/j.jes.2019.04.002.
35. Ansari, S.A., Khan, M.M., Ansari, M.O. and Cho, M.H., "Nitrogen-doped titanium dioxide (n-doped TiO_2) for visible light photocatalysis", ***New Journal of Chemistry***, Vol. 40, No. 4, (2016), 3000-3009. doi: 10.1039/C5NJ03478G.
36. Houmard, M., Riassetto, D., Roussel, F., Bourgeois, A., Berthome, G., Joud, J. and Langlet, M., "Morphology and natural wettability properties of sol–gel derived TiO_2– SiO_2 composite thin films", ***Applied Surface Science***, Vol. 254, No. 5, (2007), 1405-1414. doi: 10.1016/j.apsusc.2007.06.072.
37. Zangeneh, H., Zinatizadeh, A.A., Feyzi, M., Zinadini, S. and Bahnemann, D.W., "Photomineralization of recalcitrant wastewaters by a novel magnetically recyclable boron doped-TiO_2- SiO_2 cobalt ferrite nanocomposite as a visible-driven heterogeneous photocatalyst", ***Journal of Environmental Chemical Engineering***, Vol. 6, No. 5, (2018), 6370-6381. doi: 10.1016/j.jece.2018.10.001.
38. Namkhang, P., An, W.-J., Wang, W.-N., Rane, K.S., Kongkachuichay, P. and Biswas, P., "Low temperature synthesis of n-doped TiO_2 nanocatalysts for photodegradation of methyl orange", ***Journal of Nanoscience and Nanotechnology***, Vol. 13, No. 3, (2013), 2376-2381. doi: 10.1166/jnn.2013.7087 .
39. Rosales, A., Ortiz-Frade, L., Medina-Ramirez, I.E., Godínez, L.A. and Esquivel, K., "Self-cleaning of SiO_2- TiO_2 coating: Effect of sonochemical synthetic parameters on the morphological, mechanical, and photocatalytic properties of the films", ***Ultrasonics Sonochemistry***, Vol. 73, (2021), 105483. doi: 10.1016/j.ultsonch.2021.105483.
40. Wan, H., Yao, W., Zhu, W., Tang, Y., Ge, H., Shi, X. and Duan, T., "Fe-n co-doped SiO_2@ TiO_2 yolk-shell hollow nanospheres with enhanced visible light photocatalytic degradation", ***Applied Surface Science***, Vol. 444, (2018), 355-363. doi: 10.1016/j.apsusc.2018.03.016.
41. Bharti, B., Barman, P. and Kumar, R., "Xrd analysis of undoped and fe doped TiO_2 nanoparticles by williamson hall method", in AIP Conference Proceedings, AIP Publishing LLC. Vol. 1675, (2015), 030025, doi: 10.1063/1.4929241.
42. Habeeb, S.A., Hammadi, A.H., Abed, D. and Al-Jibouri, L.F., "Green synthesis of metronidazole or clindamycin-loaded hexagonal zinc oxide nanoparticles from ziziphus extracts and its antibacterial activity", ***Pharmacia***, Vol. 69, No. 3, (2022), 855-864. doi: 10.3897/pharmacia.69.e91057.
43. Wei, M., Song, N., Li, F., Qi, Z.-n. and Yao, M.-m., "Efficient photodegradation of organic pollutants with co–b codoped TiO_2/ SiO_2 composite films under visible light irradiation", ***Journal of Materials Science: Materials in Electronics***, Vol. 28, No. 8, (2017), 6320-6327. doi: 10.1007/s10854-016-6315-2.
44. Rasoulnezhad, H., Hosseinzadeh, G. and Yekrang, J., "Preparation and characterization of nanostructured s and fe co-doped TiO_2 thin film by ultrasonic-assisted spray pyrolysis method", ***Journal of Nanostructures***, Vol. 8, No. 3, (2018), 251-258. doi: 10.22052/JNS.2018.03.4.
45. Hosseini, O., Zare-Shahabadi, V., Ghaedi, M. and Azqhandi, M.A., "Experimental design, rsm and ann modeling of tetracycline photocatalytic degradation using LDH@ CN", ***Journal of Environmental Chemical Engineering***, Vol. 10, No. 5, (2022), 108345. doi: 10.1016/j.jece.2022.108345.
46. Reza, K.M., Kurny, A. and Gulshan, F., "Parameters affecting the photocatalytic degradation of dyes using TiO_2: A review", ***Applied Water Science***, Vol. 7, No. 4, (2017), 1569-1578. doi: 10.1007/s13201-015-0367-y.
47. Shaojun, J., Zheng, S., Daqiang, Y., Lianhong, W. and Liangyan, C., "Aqueous oxytetracycline degradation and the toxicity change of degradation compounds in photoirradiation process", ***Journal of Environmental Sciences***, Vol. 20, No. 7, (2008), 806-813. doi: 10.1016/S1001-0742(08)62130-0.
48. Balarak, D., Mengelizadeh, N., Rajiv, P. and Chandrika, K., "Photocatalytic degradation of amoxicillin from aqueous solutions by titanium dioxide nanoparticles loaded on graphene oxide", ***Environmental Science and Pollution Research***, Vol. 28, No. 36, (2021), 49743-49754. doi: 10.1007/s11356-021-13525-1.

Persian Abstract

چکیده

برای بررسی مزایای سیستم نانوکامپوزیت $Fe-N-SiO_2/TiO_2$، تخریب فوتوکاتالیستی آنتی بیوتیک اکسی تتراسایکلین (OTC) توسط TiO_2 و کامپوزیت های اصلاح شده آن با ترکیب هر یک از دوپنت ها شامل Fe، N و SiO_2 تحت شرایط خاصی مورد بررسی قرار گرفتند. خواص ساختاری و نوری و همچنین مورفولوژی نانوکامپوزیت‌های تهیه‌شده نیز با استفاده از طیف (FT-IR)، پراش اشعه ایکس، طیف سنجی فوتولومینسانس، طیف‌های DRS و FESEM/EDX مشخص شد. به منظور توسعه دو مدل که روابط عملکردی مناسب بین دو پاسخ اصلی (بازده حذف OTC و سرعت حذف ویژه آن (SRR)) و چهار متغیر عددی (غلظت OTC، غلظت کاتالیست، pH اولیه و زمان واکنش) را نشان می‌دهند، دو مسیر تجزیه و تحلیل چند متغیره مجزا تحت روش سطح پاسخ (RSM) بکار گرفته شد. نتایج به‌دست‌آمده همگی به حداکثر SRR 220) OTC mg OTC removed/g cat. h) در حداکثر دوز کاتالیزور ۱.۵ گرم در لیتر و pH اسیدی ۳ پس از ۰.۵ ساعت کاهش یافت. علاوه بر این، $Fe-N-SiO_2/TiO_2$ یک فعالیت فوتوکاتالیستی پایدار را در طی سه آزمایش پشت سر هم ثابت کرد و پتانسیل قابل اعتماد آن را برای کاربردهای آینده روشن کرد.